Cell Transplantation
2019, Vol. 28(11) 1358–1372

DOI: 10.1177/0963689719867285
journals.sagepub.com/home/cll

The Neuroprotective Effects of Necrostatin-1 on Subarachnoid Hemorrhage in Rats Are Possibly Mediated by Preventing Blood–Brain Barrier Disruption and RIP3-Mediated Necroptosis

Jingsen Chen[1,*], Hanghuang Jin[1,2,*], Hangzhe Xu[1,*], Yucong Peng[1], Liyong Jie[3], Demin Xu[4], Lili Chen[5], Tao Li[1], Linfeng Fan[1], Pingyou He[1], Guangyu Ying[1], Chi Gu[1], Chun Wang[1], Lin Wang[1], and Gao Chen[1]

Abstract

Despite the substantial efforts to elucidate the role of early brain injury in subarachnoid hemorrhage (SAH), an effective pharmaceutical therapy for patients with SAH continues to be unavailable. This study aims to reveal the role of necroptosis after SAH, and explore whether the disruption of the blood–brain barrier (BBB) and RIP3-mediated necroptosis following SAH in a rat SAH model are altered by necrostatin-1 via its selective inhibition of receptor-interacting protein kinase 1 (RIP1). Sixty-five rats were used in the experiments. The SAH model was established using endovascular perforation. Necrostatin-1 was intracerebroventricularly injected 1 h before SAH induction. The neuroprotective effects of necrostatin-1 were evaluated with multiple methods such as magnetic resonance imaging (MRI) scanning, immunohistochemistry, propidium iodide (PI) labeling, and western blotting. Pretreatment with necrostatin-1 attenuated brain swelling and reduced the lesion volume on T2 sequence and ventricular volume on MRI 72 h after SAH induction. Albumin leakage and the degradation of tight junction proteins were also ameliorated by necrostatin-1 administration. In addition, necrostatin-1 decreased the number of PI-positive cells in the basal cortex, reduced the levels of the RIP3 and MLKL proteins, and inhibited the production of the pro-inflammatory cytokines IL-1β, IL-6, and TNF-α. Based on the findings from the present study, the selective RIP1 inhibitor necrostatin-1 functioned as a neuroprotective agent after SAH by attenuating brain swelling and BBB disruption. Moreover, the necrostatin-1 pretreatment prevented SAH-induced necroptosis by suppressing the activity of the RIP3/MLKL signaling pathway. These results will provide insights into new drugs and pharmacological targets to manage SAH, which are worth further study.

Keywords

subarachnoid hemorrhage, early brain injury, necroptosis, necrostatin-1, blood–brain barrier

[1] Department of Neurosurgery, Second Affiliated Hospital, School of Medicine, Zhejiang University, Hangzhou, China
[2] Department of Neurosurgery, Affiliated Taizhou Municipal Hospital, Taizhou University, Taizhou, China
[3] Department of Radiology, Second Affiliated Hospital, School of Medicine, Zhejiang University, Hangzhou, China
[4] Department of Radiology, Peking University Shenzhen Hospital, Shenzhen, China
[5] Department of Neurology, Xiasha Campus, Sir Run Run Shaw Hospital, School of Medicine, Zhejiang University, Hangzhou, China
[*] All the authors contributed equally to this article.
[**] This article was originally submitted for Cerebrovascular Disorders issue.

Submitted: June 19, 2019. Revised: June 29, 2019. Accepted: July 11, 2019.

Corresponding Author:
Gao Chen, Department of Neurosurgery, The Second Affiliated Hospital, School of Medicine, Zhejiang University, Jiefang Road 88th, Hangzhou 310016, China.
Email: d-chengao@zju.edu.cn

Introduction

Subarachnoid hemorrhage (SAH), which is generally caused by the rupture of an intracranial aneurysm, is included in the category of fatal stroke. Patients who suffer an SAH inevitably have a high mortality rate, and delayed neurological deficits if they survive[1,2]. According to recent studies, early brain injury (EBI) is a major factor that worsens the outcome of SAH[3–5]. The possible mechanisms of EBI mainly include a sudden increase in the intracranial pressure coupled with a decrease in cerebral blood flow. This combination induces cell death, leading to a disruption of the blood–brain barrier (BBB) integrity and cerebral edema. Currently, an effective pharmaceutical therapy for patients with SAH is unavailable. Thus, novel pharmacotherapies or targets of treatment that ameliorate EBI in patients with SAH must be developed.

Programmed cell death (PCD), which plays an essential role in the pathological processes occurring after stroke, has become a hot topic in recent years. Three main types of PCD have been identified: apoptosis, autophagic cell death, and programmed necrosis. Programmed necrosis, which was also named necroptosis by Degterev et al.[6], is a caspase-independent form of PCD that is mediated by pharmaceutical interventions. Currently, necroptosis has been reported in various models of brain injury, such as ischemic brain injury, intracranial hemorrhage, neurodegenerative disease, and traumatic brain injury (TBI)[6–10]. Degterev and colleagues also identified a small-molecule inhibitor of necroptosis named necrostatin-1[6], which was characterized by its selective inhibitory effect on the receptor-interacting protein kinase 1 (RIP1)[11]. Numerous studies have recently discovered the neuroprotective effects of necrostatin-1. These beneficial effects include decreasing the brain injury volume, improving neurological functions, reducing production of reactive oxygen species, and exerting anti-neuroinflammatory, anti-endoplasmic reticulum stress, anti-apoptotic and anti-autophagic effects[12–16]. Meanwhile, several studies have explored the neuroprotective effects of necrostatin-1 at different time points after SAH, namely, at 24 h and 48 h[17–19], and have indicated a role for necroptosis after SAH. Nevertheless, to our knowledge, the evidence that necroptosis occurs after SAH is scarce, and the potential mechanisms by which necrostatin-1 protects the BBB have not yet been identified. In addition, the effects of necrostatin-1 at 72 h or a later time point after SAH have not yet been elucidated.

Brain edema, BBB disruption, and neuroinflammation are the main components of central nervous system injury, and global edema is recognized to be one of the independent predictors of an unfavorable prognosis of SAH[20]. In fact, vasogenic edema is directly caused by BBB disruption[21,22]. Although hundreds of studies have examined necrostatin-1, its potential effects on attenuating brain edema by ameliorating BBB disruption have not been completely elucidated.

Taken together, we hypothesized that necroptosis might be a potential therapeutic target for SAH. In this article, we used a rat endovascular filament model and magnetic resonance imaging (MRI) scanning to determine whether necrostatin-1 alleviates brain edema, decreases ventricular and lesion volumes, ameliorates BBB disruption, or suppresses necroptosis within the first 72 h after SAH onset.

Materials and Methods

Animals and Study Design

Adult Sprague-Dawley rats weighing 300–320 g from SLAC Laboratory Animal Co., Ltd. (Shanghai, China) were used as animal models. Housing conditions of the rats were standardized by controlling the temperature and humidity control and maintaining a 12 h light/dark cycle. All animal experiments were approved by the Ethics Committee of Zhejiang University and the relevant procedures were performed in compliance to the NIH guidelines for the Care and Use of Laboratory Animals. Sixty-five rats were used in this study and segregated into the following groups: Sham group ($n = 14$), SAH + vehicle group ($n = 26$), and SAH + Nec-1 group ($n = 25$). In the SAH + vehicle group, the endovascular perforation surgery was preceded by a vehicle pretreatment. The SAH + Nec-1 group was pretreated with Nec-1 before SAH surgery. The sham group underwent the same procedure as the SAH + vehicle group except for intracranial arterial perforation. Based on previous studies[8,13,23,24] and our unpublished data regarding the time course of changes in the levels of the RIP3 and the mixed lineage kinase domain-like (MLKL) proteins after SAH, 72 h after SAH onset was chosen as the only endpoint throughout the experiment. We used six animals per group for MRI scanning, measurements of protein levels and matrix metalloproteases (MMP) activity; six animals per group were used for propidium iodide (PI) labeling, and another two animals per group were used for immunohistochemistry and immunofluorescence staining. The deceased animals that did not complete the indicated studies were removed from the groups and replaced with new, randomly selected rats to ensure the same number of animals in each group.

Experimental Induction of SAH

Two experienced investigators induced SAH in rats via endovascular perforation, according to a previous study[25]. Pentobarbital (40 mg/kg) was intraperitoneally injected to induce deep anesthesia in rats. Briefly, after dissection and distal transection of the external carotid artery (ECA), a blunted 4-0 monofilament nylon suture was advanced from the stump of the ECA into the internal carotid artery (ICA) until resistance was sensed. The suture was then inserted 2–3 mm further to penetrate the artery wall of the intracranial bifurcation of the ICA. In the sham operation, the surgery was terminated once resistance emerged.

Drug Administration

Necrostatin-1 was purchased from Selleck Chemicals (Houston, TX, USA) and dissolved in 1% DMSO in sterile saline. Three microliters of Nec-1 (1 μg) were administered 1 h before SAH induction via a left intracerebroventricular injection at an infusion rate of 0.5 μl/min. The dosage and timing of the necrostatin-1 pretreatment were based on previous studies[26,27]. In the sham and SAH + vehicle groups, the same volume of vehicle was infused via the same route at the same time point. Details of the intracerebroventricular injection procedure are described in a previous study[28]. After the induction of anesthesia via an intraperitoneal injection of pentobarbital (40 mg/kg), a small burr hole was created with a drill, and the needle of a 10 μl Hamilton syringe (Microliter701; Hamilton Company, Reno, NV, USA) was inserted at the following coordinates: 1.5 mm posterior, 1.0 mm lateral, and 3.5 mm depth relative to the bregma. The syringe was withdrawn 10 min after the injection, and the burr hole was sealed with bone wax.

Evaluation of the Neurological Score and SAH Grade

The neurological scores were graded using a previously reported protocol[29] at different time points, namely, at 24, 48, and 72 h after SAH induction. The evaluation system was composed of six tests: spontaneous activity, symmetry in limb movement, forepaw outstretching, climbing, body proprioception, and the response to a touch of the vibrissae. Each test was scored as either 0–3 or 1–3 points, and the total scores ranged from 3 to 18 points. The behavioral tasks were administered to the animals in a random sequence. After the rats were euthanized, the SAH score was quantified using a previously described SAH grading system[30]. The subarachnoid blood clots were observed over the basal cistern, which was divided into six parts based on its anatomy. Each segment received a score of 0 to 3 points, depending on the degree of bleeding, with the summary ranging from 0 to 18 points. All evaluations and grading processes were conducted by an independent observer, and the animals were evaluated in a random order. Animals with an SAH grade less than 6 were excluded from this study and replaced with new, randomly selected rats to ensure the same numbers of animals in each group.

MRI and Measurements

MRI was performed with a 3.0-T GE Discovery MR750 scanner (General Electric Company, Boston, MA, USA) 72 h after SAH. T2 fast spin-echo sequences were scanned in each rat using a field of view of 60 × 60 mm, a matrix of 256 × 256 and 9 coronal slices (2 mm thick). All the MRI data were analyzed by an independent researcher using NIH ImageJ software. Brain swelling was measured in images of nine sections as described in a previous publication[31], and the values were calculated as follows: ((volume of the left hemisphere – volume of the right hemisphere)/volume of the right hemisphere) × 100%[32]. Ventricular volume was determined using the method reported in a previous study[33] and was measured from the frontal horn of the lateral ventricle to the lateral aperture of the fourth ventricle using the formula $\Sigma(A_n + A_{n+1}) \times d/2$, where A represents the ventricular area and d the distance between sections. The lesion volume on T2 sequences was confirmed as described in a previous study[34]. Briefly, a pixel was considered abnormal if its value exceeded two standard deviations of the mean value of the contralateral hemisphere, and the result is presented as a ratio of the volume of the ipsilateral hemisphere.

Western Blot Analysis

Western blotting was conducted using our previously reported protocol[35]. At 72 h after modeling, the rats were deeply anesthetized and transcardially perfused with PBS (0.1 mol/l, pH 7.4). The brains were removed, and the left basal cortices adjacent to blood clots were dissected, weighed, and homogenized. The samples were centrifuged at 1000 *g* for 10 min at 4°C. The supernatants were further centrifuged, and a detergent-compatible protein assay kit (Bio-Rad, Hercules, CA, USA) was used to measure the protein concentration. Equivalent amounts of samples (40 μg) were resuspended in loading buffer and heated at 100°C for 5 min. The samples and molecular markers were then loaded on the gel and separated using sodium dodecyl sulfate polyacrylamide gel electrophoresis (SDS-PAGE). Afterwards, proteins were transferred from the gel to a polyvinylidene difluoride (PVDF) membrane. After blocking the nonspecific binding with 5% skim milk for 2 h, membranes were incubated overnight at 4°C on a shaker with the following primary antibodies: albumin (1:5000, Bethyl Laboratories, Montgomery, TX, USA Cat# A90-134A), ZO-1 (1:2000, Santa Cruz Biotechnology, Santa Cruz, CA, USA, Cat# SC-10804), Occludin (1:2000, Santa Cruz Biotechnology, Cat# SC-5562), Claudin-5 (1:800, Santa Cruz Biotechnology, Cat# SC-28670), MMP-9 (1:5000, Abcam, Cambridge, MA, USA, Cat# ab38898), RIP3 (1:1000, Novus Biologicals, Littleton, CO, USA, Cat# NBP1-77299), MLKL (1:500, Santa Cruz Biotechnology, Cat# SC-165025), caspase-8 (1:3000, Abcam, Cat# ab25901), IL-1β (1:800, Santa Cruz Biotechnology, Cat# SC-23459), IL-6 (1:2500, Abcam, Cat# ab9324), TNF-α (1:1000, Abcam, Cat# ab6671), and β-actin (1:5000, Abcam, Cat# ab8226). Next, membranes were incubated with the appropriate secondary antibodies (1:5000) for 1 h at room temperature. The bands were visualized using X-ray film and analyzed by densitometry using ImageJ software (NIH). The levels of target proteins were normalized to the levels of the structural protein to ensure comparability of the results between groups.

Gelatin Zymography

Gelatin zymography was performed using an MMP zymography assay kit (Applygen Technologies, Beijing, China, Cat# P1700) as described in a previous study[36]. Equivalent amounts of the prepared protein samples (40 μg) were loaded and separated on a 10% Tris-glycine gel containing 0.1% gelatin as a substrate. After electrophoresis, the gels were placed in 2.5% Triton X-100 for 1 h to remove the SDS and then incubated at 37°C for 24 h with developing buffer. Then, the gels were stained with 0.5% Coomassie Blue R-250 for 2 h and then destained. The intensities of the proteolyzed bands indicated gelatinase activity. The intensity of zymography bands was measured and analyzed using Quantity One software (Bio-Rad).

Propidium Iodide (PI) Labeling

At 71 h after SAH induction, PI (Sigma-Aldrich, St. Louis, MO, USA) diluted to 10 mg/ml in sterile saline was injected intraperitoneally at a dose of 30 mg/kg. One hour later, the rats underwent transcardial perfusion with 0.1 mol/l PBS (pH 7.4) followed by 4% paraformaldehyde (pH 7.4). Then, the brains were harvested, fixed with 4% formaldehyde for 48 h at 4°C, and then dehydrated with a 30% sucrose solution until the brain samples sank to the bottom of the vessel (approximately 2–3 days). After fixation, the brains were embedded into tissue-freezing media and cut into coronal frozen sections (7 μm) at 150–200 μm intervals near the optic chiasma. PI-positive cells were counted in 200 × fields of the left basal cortex in three different sections per rat using a fluorescence microscope (Olympus, Tokyo, Japan). An independent observer counted the cells.

Immunohistochemistry

Immunohistochemistry was performed as described in a previous study[37]. Rats were euthanized 72 h after SAH induction and transcardially perfused with 0.1 mol/l PBS (pH 7.4) followed by 4% paraformaldehyde (pH 7.4) as described above. Then, the brains were removed, fixed, dehydrated, and cut into coronal frozen sections (7 μm). The sections were incubated with a goat anti-mouse albumin antibody (1:500, Bethyl Laboratories, Cat# A90-134A) at 25°C for 2 h and washed with PBS (pH 7.4). After the sections were further incubated with secondary antibody for an additional 1 h at 25°C, the reaction product was visualized using a DAB peroxidase substrate kit SK-4100 (Vector Laboratories, Burlingame, CA, USA). An Olympus BX41 microscope was used to capture the images.

Immunofluorescence Staining

At 72 h after SAH induction, the rats were sacrificed and transcardially perfused with 0.1 mmol PBS (pH 7.4). Brain tissues were removed, fixed with 4% formaldehyde for 48 h at 4°C and then dehydrated with a 30% sucrose solution until the brain samples sank to the bottom of the vessel (approximately 2–3 days). After fixation and embedding in tissue-freezing media, the frozen brain tissues were cut into coronal sections (7 μm) at 150–200 μm intervals near the optic chiasma. The brain sections were preprocessed for 60 min in 0.01 mmol PBS (pH 7.4) containing 10% normal serum consistent with the species of the secondary antibody and 0.3% Triton X-100 to prevent nonspecific binding. Then, the brain sections were incubated overnight at 4°C with the following primary antibodies: Claudin-5 (1:100, Santa Cruz Biotechnology, Cat# SC-28670), RIP3 (1:250, Cell Signaling Technology, Danvers, MA, USA, Cat# 95702 s), and caspase-3 (1:200, Cell Signaling Technology, Cat# 9668s). After several washes with PBS, the sections were incubated with secondary antibodies for 2 h at 4°C in the dark. Then, the sections were rinsed and mounted onto slides with Fluoroshield™ containing DAPI (Sigma-Aldrich, Cat# F6057). Immunostaining was observed using a fluorescence microscope (Olympus).

Statistical Analysis

Western blot results from the three groups are described as the relative density of the target proteins normalized to β-actin and then compared with the sham group. The data are presented as the means ± SEM. Statistically significant differences between each pair of groups were analyzed using one-way analysis of variance (ANOVA) followed by Tukey's multiple comparison test. A value of $p < 0.05$ was regarded as statistically significant. All statistical analyses were performed using SPSS (version 22.0 IBM, Armonk, NY, USA) and Prism (version 6.0) statistical software.

Results

Neurological Scores, SAH Grade, and Mortality

Representative images of brain samples from each group are presented in Fig. 1A. The induction of SAH significantly decreased the neurological scores compared with the sham group at 24, 48, and 72 h after SAH ($p < 0.05$ compared with the SAH + vehicle group, Fig. 1B). Pretreatment with Nec-1 significantly ameliorated the neurological deficits at each time point after SAH ($p < 0.05$ compared with the SAH + vehicle group, Fig. 1B). The statistical diagrams of detailed scores of each neurological test are shown in the supplementary file. SAH scores of the SAH + Nec-1 group were not significantly different from the SAH + vehicle group ($p > 0.05$, Fig. 1C). The mortality of each group was sham group 0% (0/14), SAH + vehicle group 46.2% (12/26) and SAH + Nec-1 group 44% (11/25). The pharmacological intervention in the SAH + Nec-1 group failed to significantly alter mortality ($p > 0.05$ compared with the SAH + vehicle group, Fig. 1D).

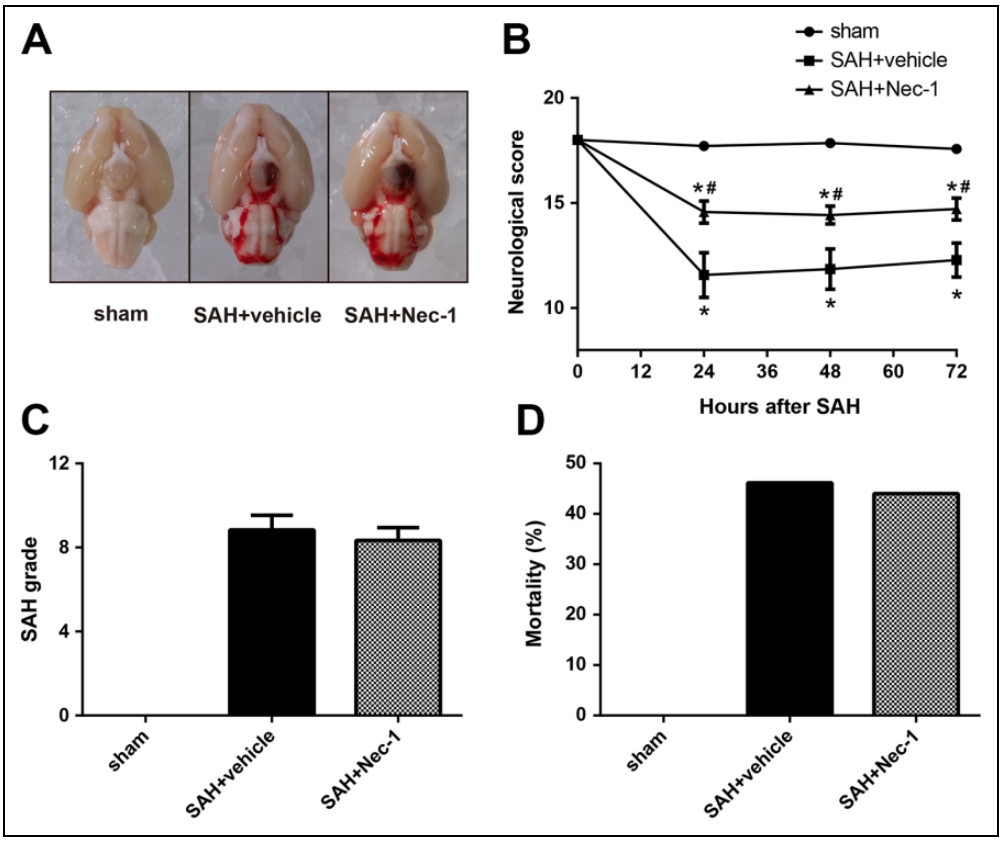

Figure 1. Representative images of brain samples from each group and neurological scores, SAH grade and mortalities at 72 h after SAH. (a) Typical brains from sham, SAH + vehicle, and SAH + Nec-1 group. (b) The quantification of neurological scores in 24, 48, and 72 h after SAH induction. (c) The quantification of SAH severity. (d) The quantification of mortality. The bars represent the mean ± SEM. $n = 14$. $^{*}p < 0.05$ versus sham, $^{\#}p < 0.05$ versus SAH + vehicle.

Necrostatin-1 Attenuated Brain Swelling, Reduced the Lesion Volume and Ventricular Volume on T2 Sequences after SAH

Representative MRI T2 images from each group are shown in Fig. 2A. Seventy-two hours after SAH, a remarkable increase in the brain swelling index was observed in the ipsilateral hemisphere compared with the sham group ($p < 0.05$, Fig. 2B). The necrostatin-1 pretreatment significantly attenuated the swelling of the left hemisphere at 24 h ($p < 0.05$ compared with the SAH + vehicle group, Fig. 2B). No lesions were observed on T2 images of the ipsilateral hemisphere in the sham group, while obvious lesions were noted in the SAH + vehicle group (Fig. 2A). Compared with the lesions in the SAH + vehicle group, the necrostatin-1 pretreatment significantly decreased the lesion volume caused by SAH on T2 sequences ($p < 0.05$, Fig. 2C). SAH induced a significant ventricular enlargement ($p < 0.05$ compared with the sham group, Fig. 2D), which was ameliorated by the application of Nec-1 ($p < 0.05$ compared with the SAH + vehicle group, Fig. 2D).

Necrostatin-1 Decreased Albumin Leakage after SAH

Immunohistochemistry and western blotting were performed to evaluate the BBB disruption. Representative images of albumin immunoreactivity in each group are presented in Fig. 3A. The onset of SAH significantly increased the leakage of albumin around the vessels at 72 h, whereas necrostatin-1 significantly decreased this process ($p < 0.05$ compared with the SAH + vehicle group, Fig. 3B).

Necrostatin-1 Prevented the Disruption of Tight Junction Proteins after SAH

The levels of occludin, claudin-5, and ZO-1 were detected and western blotting and immunofluorescence staining for claudin-5 was performed in each group to evaluate how the proteins constituting tight junctions were impacted by necrostatin-1 at 72 h after SAH. A significant decrease in the levels of these proteins was observed in the SAH + vehicle group, but not in sham group ($p < 0.05$, Fig. 4A–D). Necrostatin-1 significantly attenuated the degradation of occludin, claudin-5, and ZO-1($p < 0.05$ compared with the

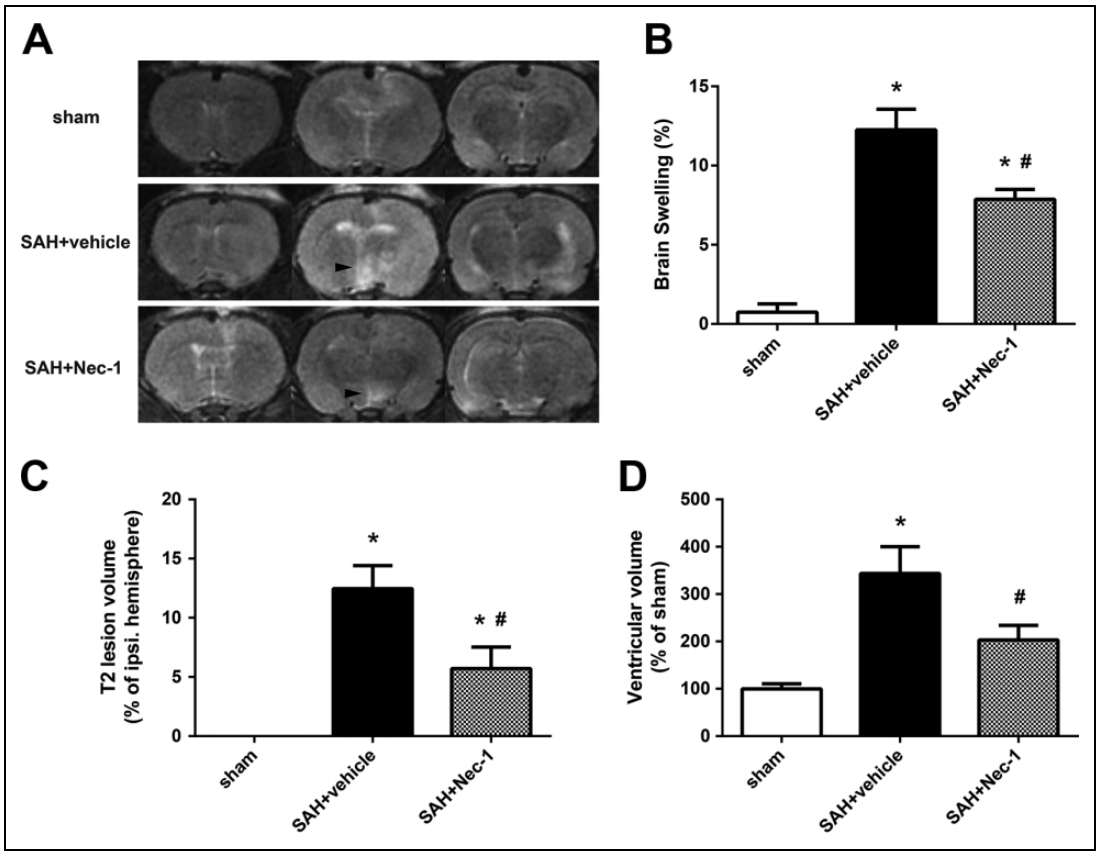

Figure 2. Necrostatin-1 attenuated brain swelling, reduced the lesion volume and ventricular volume on T2 sequences after SAH. (a) Representative T2-weighted MRI images of the brains from sham, SAH + vehicle, and SAH + Nec-1 group. (b) Brain swelling was calculated as ((volume of ipsilateral hemisphere – volume of contralateral hemisphere)/volume of contralateral hemisphere) × 100%. (c) T2 lesion volume was presented as the volume ratio to the ipsilateral hemisphere. (d) Ventricular volume was presented as the volume ratio to the average volume of the sham group. The bars represent the mean ± SEM. $n = 6$. $^{*}p < 0.05$ versus sham, $^{\#}p < 0.05$ versus SAH + vehicle.

SAH + vehicle, Fig. 4A–D). Immunofluorescence staining revealed high levels of claudin-5 in the sham group, but low levels in the SAH + vehicle group. The necrostatin-1 pretreatment visibly improved claudin-5 expression in the basal cortex of the ipsilateral hemisphere (Fig. 4E). Based on these results, necrostatin-1 attenuated the disruption of BBB integrity at 72 h post-SAH.

Necrostatin-1 Prevented the SAH-Induced Increase in MMP-9 Levels and Activity

The impairment of the BBB caused by the degradation of tight junction components after stroke might be mediated by MMPs[38], particularly MMP-9[39]. SAH induction significantly increased MMP-9 levels ($p < 0.05$ compared with the sham group, Fig. 5A and C), changes that were counteracted by the pretreatment with necrostatin-1 ($p < 0.05$ compared with the SAH + vehicle group, Fig. 5A and C). Gelatin zymography revealed a significant increase in MMP-9 proteolytic activity at 72 h in the SAH + vehicle group ($p < 0.05$ compared with the sham group, Fig. 5B and D), which was also counteracted by the pretreatment with necrostatin-1 ($p < 0.05$ compared with the SAH + vehicle group, Fig. 5B and D). However, the proteolytic activity of MMP-2 did not change significantly among each group (Fig. 5B and E).

Necrostatin-1 Decreased the Number of PI-Positive Cells after SAH

With the aim of evaluating the effect of necrostatin-1 on protecting cells from injury, PI was used to identify the ruptured cells. The number of PI-positive cells was significantly increased in the basal cortex of the ipsilateral hemisphere at 72 h after SAH ($p < 0.05$ compared with the sham group, Fig. 6A and B), but the value was significantly decreased by the pretreatment with necrostatin-1 ($p < 0.05$ compared with the SAH + vehicle group, Fig. 6A and B).

Necrostatin-1 Decreased the Activity of the RIP3/MLKL Signaling Pathway after SAH

We performed double immunofluorescence staining for RIP3 and caspase-3 to distinguish cellular necroptosis from apoptosis. Some of the RIP3-positive cells were negative

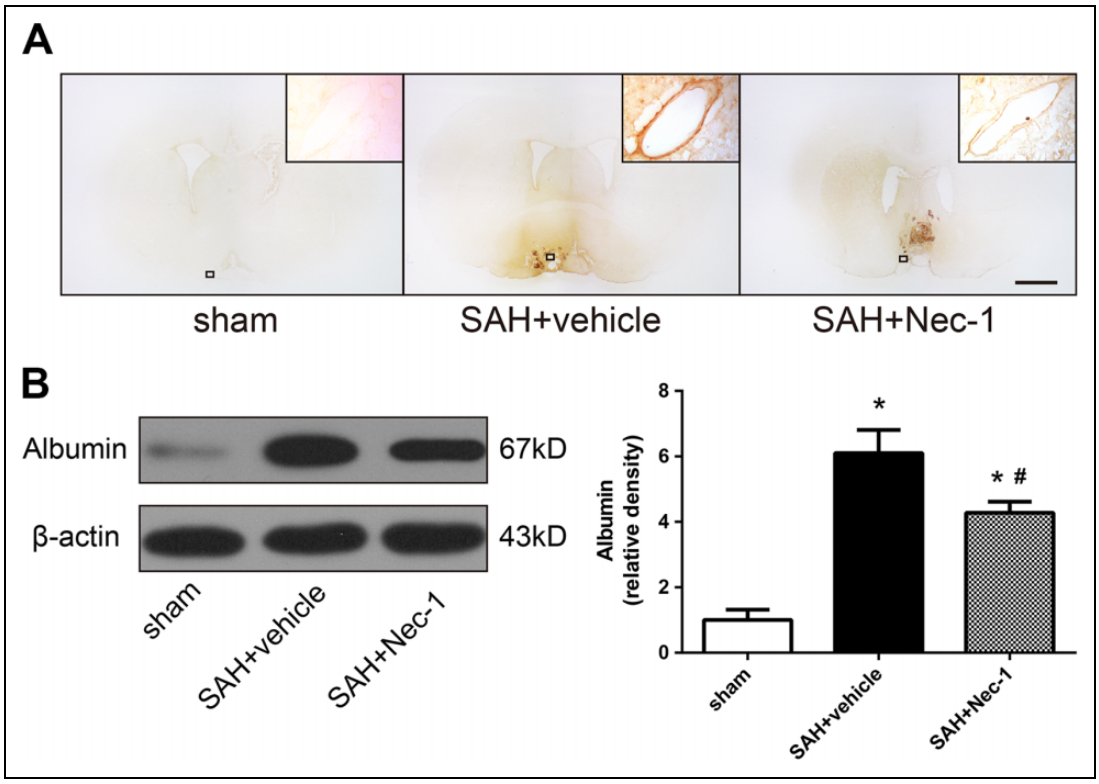

Figure 3. Necrostatin-1 decreased albumin leakage after SAH. (a) Histological panels showed the albumin immunostaining in the perivascular regions of the ipsilateral basal cortex from sham, SAH + vehicle, and SAH + Nec-1 group. (b) Western blot assay for the level of albumin in the ipsilateral basal cortex in sham, SAH + vehicle, and SAH + Nec-1 groups at 72 h after SAH induction. The bars represent the mean ± SEM. $n = 6$. *$p < 0.05$ versus sham, #$p < 0.05$ versus SAH + vehicle.

for caspase-3 (Fig. 7A). Levels of proteins involved in the RIP3/MLKL signaling pathway were also determined using western blotting to further confirm the role of necrostatin-1 in necroptosis. In the SAH + vehicle group, levels of the RIP3 and MLKL proteins were significantly increased compared with the sham group ($p < 0.05$, Fig. 7B, C and D, while necrostatin-1 administration exerted a significant inhibitory effect on the increased production of these proteins ($p < 0.05$ compared with the SAH + vehicle group, Fig. 7B, C and D). Caspase-8 suppressed the RIP1–RIP3 complex, and decreased caspase-8 levels can trigger necroptosis[40,41]. Therefore, we also examined the level of the caspase-8 protein and observed a significant decrease 72 h after SAH ($p < 0.05$ compared with the sham group, Fig. 7B and E). The necrostatin-1 pretreatment generally increased caspase-8 levels ($p < 0.05$ compared with the SAH + vehicle group, Fig. 7B and E).

Necrostatin-1 Attenuated Neuroinflammation after SAH

Several pro-inflammatory cytokines, such as IL-1β, IL-6, and TNF-α, were also identified as contributors in SAH. Necrostatin-1 suppressed the SAH-induced increase in the levels of these pro-inflammatory cytokines at 72 h ($p < 0.05$ compared with the SAH + vehicle group, Fig. 8A-D).

Discussion

In the present study, the neuroprotective effect of necrostatin-1 on experimental SAH and its potential mechanisms were explored. The necrostatin-1 pretreatment significantly improved neurological functions, decreased brain swelling and the ventricular volume, reduced lesion volume on T2 images, and attenuated the BBB disruption. Necrostatin-1 also reduced the levels of pro-inflammatory cytokines and the number of injured cells. Furthermore, the activity of the RIP3/MLKL signaling pathway was also suppressed by pretreatment with necrostatin-1.

Necrostatin-1 is the first identified small-molecule inhibitor of necroptosis[6] that targets the RIP1 kinase in the necroptosis pathway[11]. In addition, other necrostatins also target RIP1 through distinct mechanisms, such as necrostatin-3, 4, and 5. Although necrostatin-3 is less effective than necrostatin-1 in inhibiting the activity of wild-type RIP1, it still effectively inhibits the S161E mutant RIP1[11]. Necrostatin-4 exhibits a slightly higher inhibitory constant ($IC_{50} = 0.37$ μM) than necrostatin-1 ($IC_{50} = 0.32$ μM)[42], but the half-maximum response (EC_{50}) for

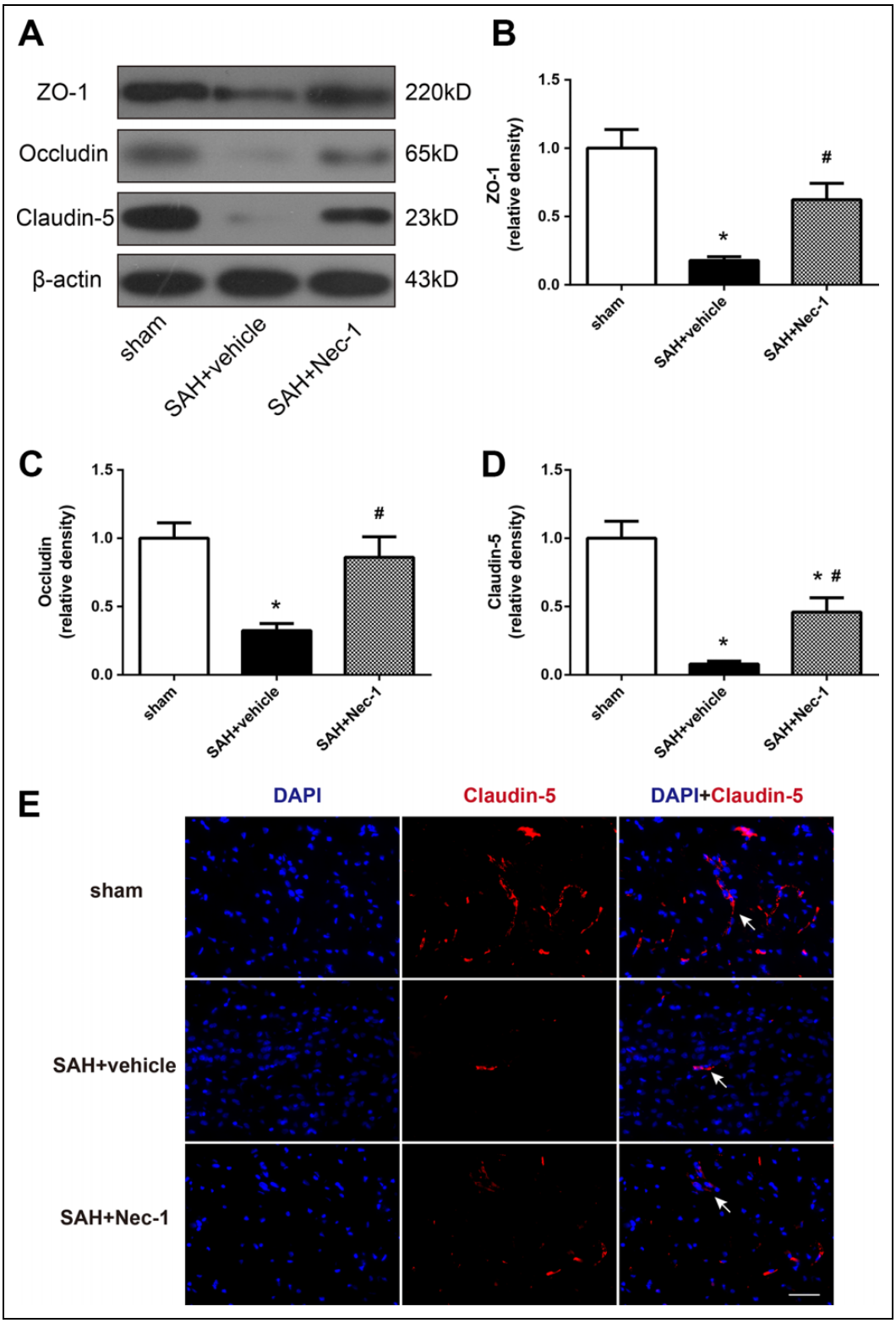

Figure 4. Necrostatin-1 Prevented the Disruption of Tight Junction Proteins after SAH. (a) Representative Western blots showing levels of ZO-1, occludin and claudin-5 in the ipsilateral cortex in each group 72 h after SAH induction. (b–d) The relative band densities of ZO-1, occluding, and claudin-5. The densities of the protein bands were analyzed and normalized to β-actin, and compared with the mean value of the sham group. The bars represent the mean ± SEM. $n = 6$. *$p < 0.05$ versus sham, $^{\#}p < 0.05$ versus SAH + vehicle. (e) Representative microphotographs of immunofluorescence staining showing the levels of claudin-5 in each group. White arrows indicate the claudin-5-positive parts. Scale bar = 50 μm.

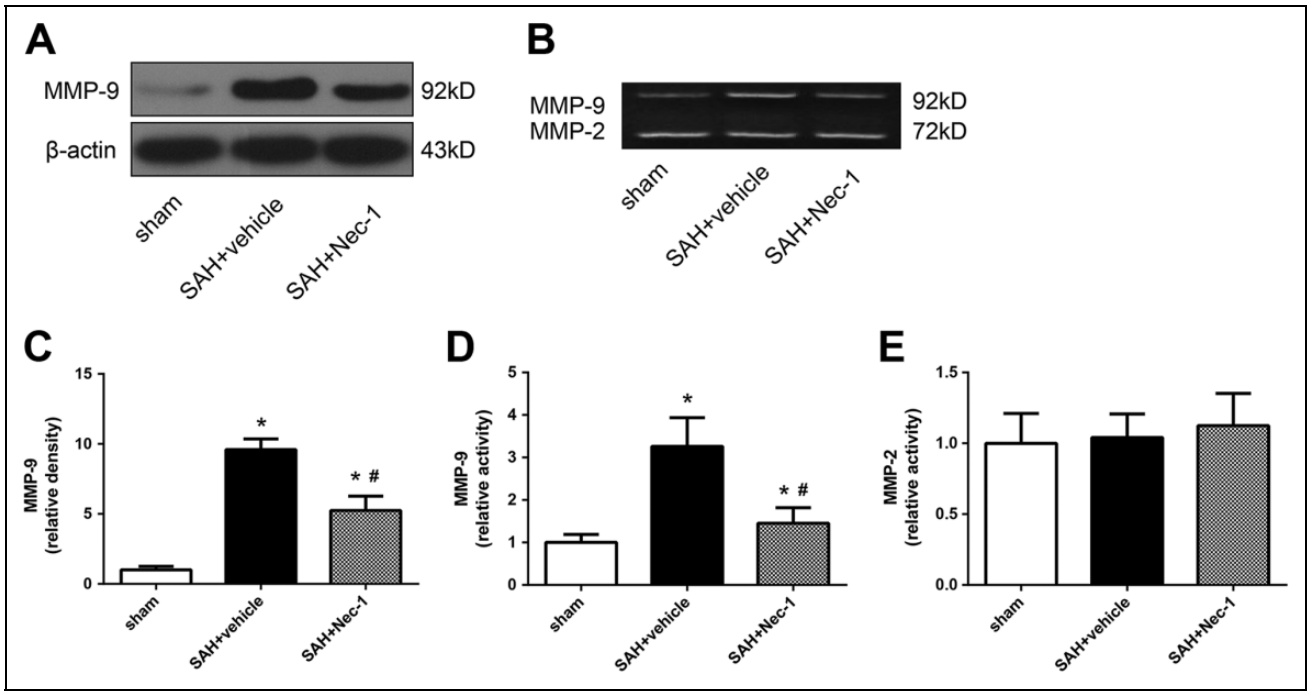

Figure 5. Effect of necrostatin-1 pretreatment on MMP-9 levels and acitvities 72 h after SAH induction. (a) Representative Western blots showing levels of MMP-9 in the ipsilateral cortex in each group 72 h after SAH induction. (b) Representative gelatin zymography bands showing activities of MMP-9 and MMP-2 in the ipsilateral cortex in each group 72 h after SAH induction. (c) The relative band densities of MMP-9. The densities of the protein bands were analyzed and normalized to β-actin, and compared with the mean value of the sham group. (d) The relative activity of MMP-9. (e) The relative activity of MMP-2. The bars represent the mean ± SEM. $n = 6$. *$p < 0.05$ versus sham, #$p < 0.05$ versus SAH + vehicle.

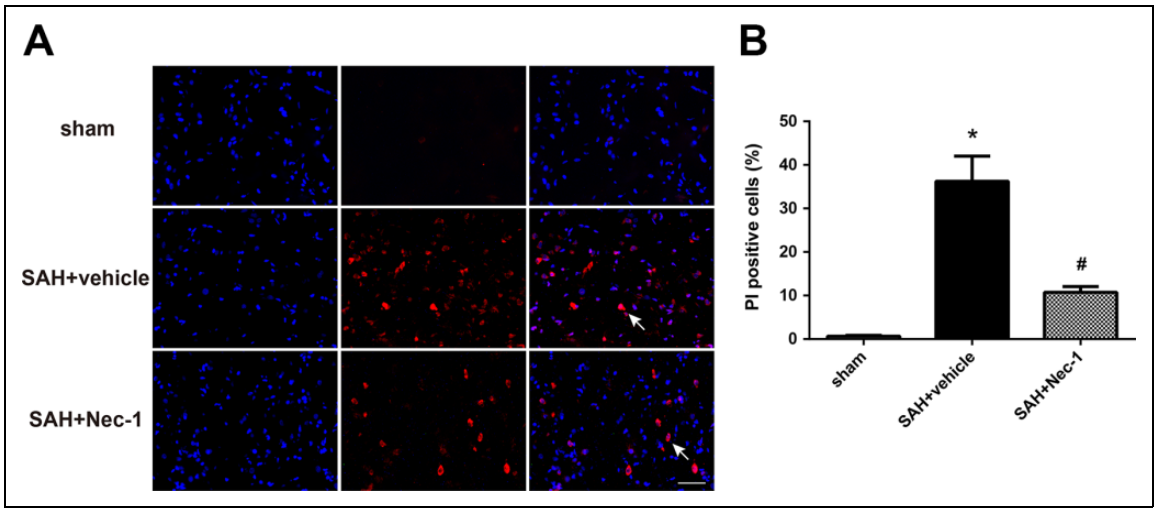

Figure 6. Effect of necrostatin-1 on cell injury in the ipsilateral basal cortex 72 h after SAH induction. (a) Representative microphotographs showed the co-localization of DAPI (blue) with PI (red) positive cells in the ipsilateral basal cortex at 72 h after SAH induction. White arrows indicate the PI-positive cells. (b) Quantitative analysis of PI-positive cells showed that necrostatin-1 could significantly reduce the percentage of PI-positive cells in the ipsilateral basal cortex at 72 h after SAH induction. The bars represent the mean ± SEM. $n = 6$. *$p < 0.05$ versus sham, #$p < 0.05$ versus SAH + vehicle. Scale bar = 50 μm.

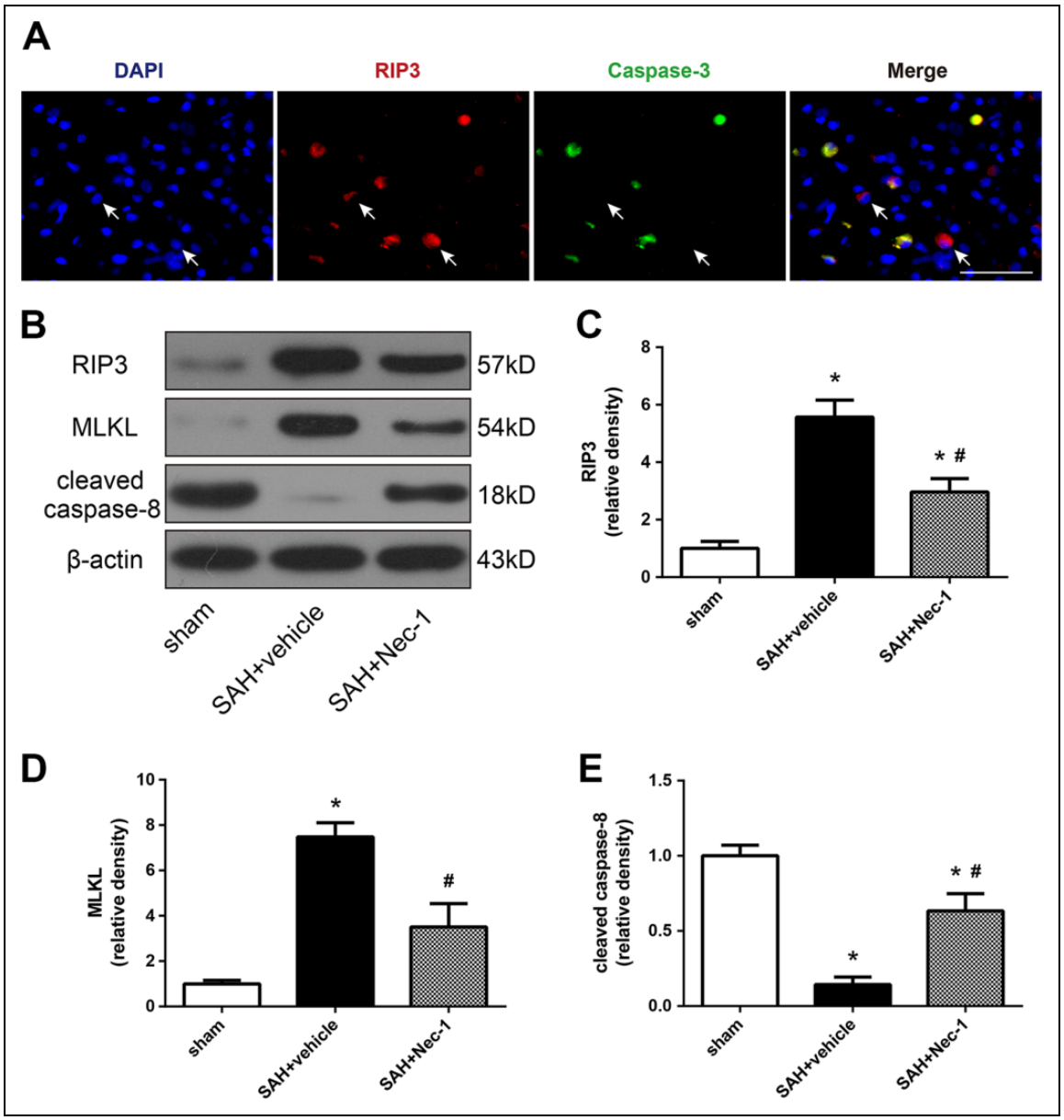

Figure 7. Necrostatin-1 down-regulated RIP3/MLKL signaling pathway after SAH induction. (a) Representative microphotographs of immunofluorescence staining showing the localization of RIP3 (green) with caspase-3 (red) in ipsilateral basal cortex at 72 h after SAH induction. White arrows indicate the RIP3-positive and caspase-3 negative cells. (b) Representative Western blots showing levels of RIP3, MLKL, and cleaved caspase-8 in the ipsilateral cortex in each group 72 h after SAH induction. (c–e) The relative band densities of RIP3, MLKL, and cleaved caspase-8. The densities of the protein bands were analyzed and normalized to β-actin, and compared with the mean value of the sham group. The bars represent the mean ± SEM. $n = 6$. $^{*}p < 0.05$ versus sham, $^{\#}p < 0.05$ versus SAH + vehicle. Scale bar = 50 μm.

necrostatin-5 (0.24 μM) exceeds the activity of necrostatin-1 (EC_{50} = 0.49 μM)[43]. In addition, another necroptosis inhibitor, necrostatin-7 (EC_{50} = 10.6 μM), does not inhibit RIP1 kinase[44]. Therefore, necrostatin-1 is still the most widely used specific inhibitor of RIP1.

SAH is a fatal disease with few effective therapeutic strategies. The rodent model of SAH using a filament for endovascular perforation is a practical animal model to simulate the pathophysiological changes after aneurysmal SAH. Brain edema, which is a major component of EBI after SAH[21] and an independent predictor of an unfavorable prognosis[20], is conducive to a series of pathological changes, such as brain swelling and neuronal cell death[22]. As shown in our previous studies, strategies that decrease the brain water content improve the neurological scores of SAH rats[45,46]. In the present study, we used a 3.0-T MRI to evaluate the brain swelling level instead of measuring the brain water content, because the former method is noninvasive and

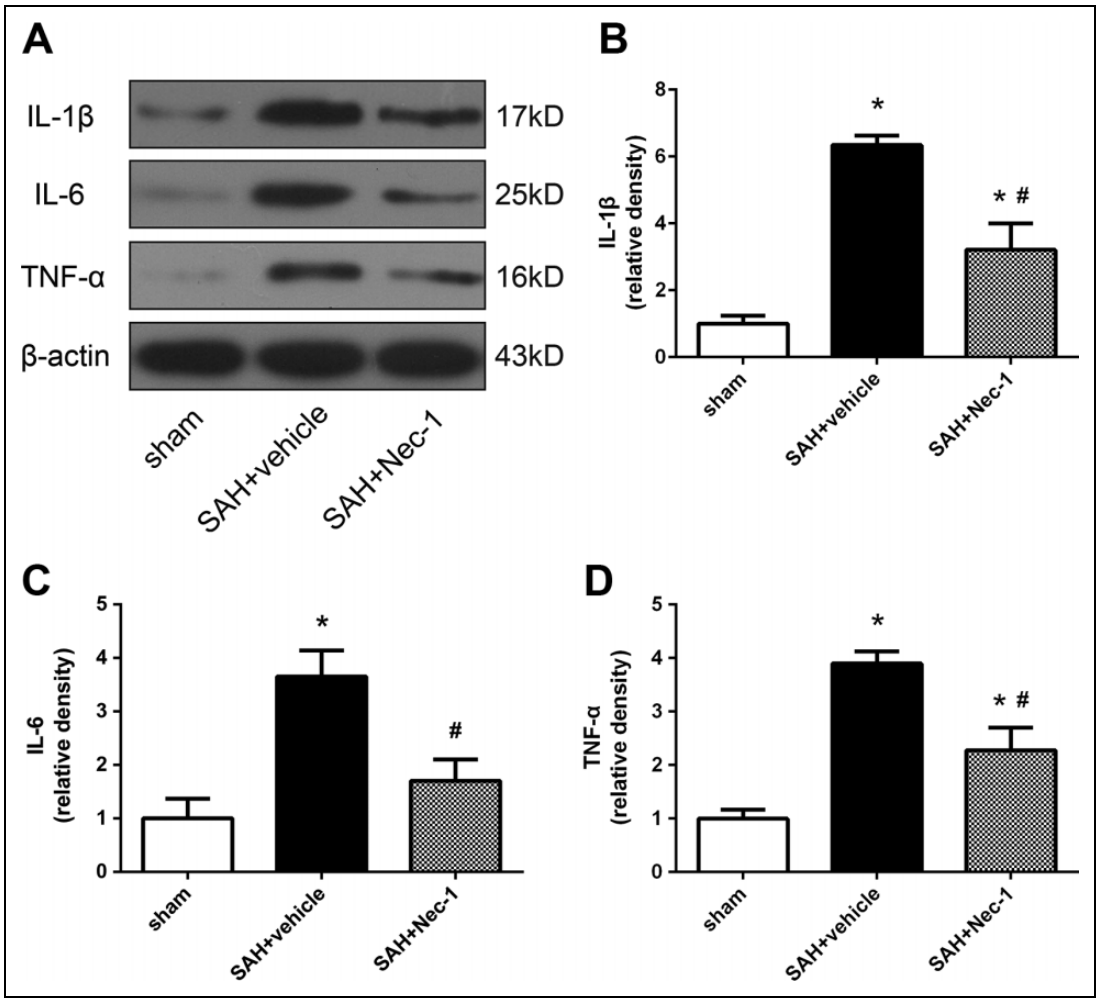

Figure 8. Necrostatin-1 attenuated neuroinflammation after SAH induction. (a) Representative western blots showing levels of IL-1β, IL-6, and TNF-α in the ipsilateral cortex in each group 72 h after SAH induction. (b–d) The relative band densities of IL-1β, IL-6, and TNF-α. The densities of the protein bands were analyzed and normalized to β-actin, and compared with the mean value of the sham group. The bars represent the mean ± SEM. $n = 6$. *$p < 0.05$ versus sham, #$p < 0.05$ versus SAH + vehicle.

could minimize animal deaths. The MRI scan also enabled us to measure the lesion volume on T2 sequences and the ventricular volumes of rats in each group. Lesion volume on T2 sequences are related to Garcia's neurological score and the MRI grading of SAH[34]. Another study examining SAH-induced hydrocephalus noted a correlation between the ventricular volume and the severity of SAH[33]. In the current study, necrostatin-1 attenuated brain swelling, and reduced lesion volumes on T2 sequences and ventricular volumes after SAH. These findings were consistent with previous studies investigating the effects of necrostatin-1 on attenuating brain edema after ischemic brain injury[23] and intracerebral hemorrhage[8]. Since vasogenic brain edema is directly caused by BBB disruption, the effect of necrostatin-1 on the BBB disruption must be determined. Based on our findings, necrostatin-1 prevented albumin leakage, indicating that it might be effective in preventing BBB disruption. We further detected the levels of tight junction proteins to identify the mechanisms underlying these findings, and necrostatin-1 prevented their degradation. In addition, necrostatin-1 also decreased the level and activity of MMP-9, which is responsible for the degradation of tight junction proteins[39] and correlates with functional outcomes after SAH[47]. These results might partially explain the neuroprotective effect of necrostatin-1.

Necroptosis is a type of necrotic cell death that depends on RIP3[48]. In this process, RIP1 interacts with RIP3 to form the necrosome[48,49]. Therefore, the RIP1 inhibitor necrostatin-1 was considered a specific inhibitor of necroptosis. Recently, a pivotal role for MLKL in RIP3-mediated necroptosis has been illustrated in multiple studies[50,51]. After phosphorylation by RIP3, MLKL forms an oligomer and directly disrupts membrane integrity[51]. In fact, both apoptosis and autophagic cell death, along with their co-relationship, have already been acknowledged in SAH in our previous study[52]. In the present study, necroptosis also

occurred after SAH, and necrostatin-1 has been reported to facilitate neuroprotection by ameliorating brain edema, BBB dysfunction, and neuroinflammation induced by SAH within the first 48 h[17]. The levels of RIP3 and MLKL were both increased 72 h after SAH, and necrostatin-1 administration significantly decreased RIP3 and MLKL levels compared with the SAH + vehicle group, thus attenuating cell injury and improving neurological function. In addition, immunofluorescence staining showed that some of the RIP3-positive cells were negative for caspase-3. These results confirmed a role for necroptosis after SAH and supported the hypothesis that necrostatin-1 ameliorated this cell death pathway, similar to other types of experimental brain injury.

Neuroinflammation occupies an important position in the pathophysiological processes of distinct insults. The connection between brain injury after SAH and the production of a series of pro-inflammatory cytokines, such as IL-1β, IL-6, and TNF-α, has been clarified by multiple studies[53–56]. RIPs, basically, may also play a necroptosis-independent role in inflammation and mediate inflammasome activation through several pathways[57]. Thus, we hypothesized that the RIP1 inhibitor necrostatin-1 might also exert an anti-inflammatory effect on EBI after SAH. The results of this study identified an effect of necrostatin-1 on preventing the upregulation of pro-inflammatory cytokines at 72 h after SAH. These results were consistent with previous studies of LPS-induced neuroinflammation[24] and intracerebral hemorrhage models[8]. In addition, inflammatory cytokines, particularly IL-1β, are considered the main activators of MMP-9[58–60], and this result also provides an explanation for the decreased levels and activity of MMP-9 observed after necrostatin-1 administration.

The blockage of cerebrospinal fluid (CSF) pathways by blood clots has been considered as the main cause of acute hydrocephalus. However, recent studies indicated that hydrocephalus may also have a relationship with inflammation[61,62], which could cause CSF hypersecretion by stimulating choroid plexus epithelium[63]. As Nec-1 could not accelerate the absorption rate of the hematoma in subarachnoid cavity (Fig. 1C), a possible explanation of Nec-1's effect of reducing ventricular volume is that it can control inflammation after SAH. However, the concrete mechanisms still need to be further explored.

In addition to necroptosis, several other types of PCD are believed to participate in EBI after SAH: apoptosis, autophagy, pyroptosis, and ferroptosis. Different types of cell death have been shown to simultaneously occur in neurons after SAH, resulting in a mixed morphologies of cell death[64]. Among these pathways, apoptosis and autophagy have been identified as two major PCD forms. The crosstalk between autophagy and apoptosis after SAH has been mainly clarified in recent years, as autophagy protects cells from apoptosis via the mitochondrial pathway[35,52]. At the same time, the relationship between necroptosis and apoptosis has also been explored by researchers. RIP1 and RIP3 contribute to both necroptosis and apoptosis, depending on the downstream effectors[65,66]. This finding might explain the coexpression of RIP3 and caspase-3 in the images of double immunofluorescence staining shown in Fig. 6A. In addition, the autophagy protein p62 is also a necessary component of the RIP1/RIP3 necrosome and controls the switch between the cell death pathways apoptosis and necroptosis[67].

Our study investigated the neuroprotective effect of necrostatin-1 on experimental SAH and discussed the potential mechanisms. However, several limitations still exist in this study. The mechanism underlying the anti-inflammatory effect of necrostatin-1 was not completely elucidated. Based on another current study from our department[18], the regulation of NLRP3 inflammasome activation might be one possible explanation. Moreover, the long-term neuroprotective effects of necrostatin-1 require further research.

Conclusions

In summary, the selective RIP1 inhibitor necrostatin-1 functions as a neuroprotective agent after SAH by attenuating brain swelling and BBB disruption. In addition, the necrostatin-1 pretreatment prevents necroptosis after SAH by suppressing the activity of the RIP3/MLKL signaling pathway. These results provide insights into new drugs and pharmacological targets to manage SAH, and thus are worth further study.

Ethical Approval

This study was approved by the Ethics Committee of Zhejiang University, China.

Statement of Human and Animal Rights

All of the experimental procedures involving animals were conducted in accordance with the Ethics Committee of Zhejiang University, China and were performed in compliance to the NIH guidelines for the Care and Use of Laboratory Animals.

Statement of Informed Consent

There are no human subjects in this article and informed consent is not applicable.

Declaration of Conflicting Interests

The author(s) declared no potential conflicts of interest with respect to the research, authorship, and/or publication of this article.

Funding

The author(s) disclose the receipt of the financial support listed below for the research, authorship, and/or publication of this article: This study was supported by grants from Key Research and Development Project of Zhejiang Province (2018C03011), the Natural Science Foundation for Young Scientists of China (81700705), the Natural Science Foundation of Zhejiang Province (LQ15H090001, LY17H070001, LY17H090007, LY17H090008 and LY19H090019), the Project of Medicine and Health of Zhejiang Province (2014KYA093), the Project of Key Medical Subject and Innovation Platform Construction of Zhejiang Province (11CX08), the Project of Chinese Medicine Science and Technology of Department of Zhejiang Province (2017ZA086), the TCM

Science and Technology Plan of Zhejiang province (2017ZZ013), and the Project of Science and Technology Plan of Hangzhou City (2014A62).

ORCID iD

Gao Chen https://orcid.org/0000-0003-1085-0028

Supplemental Material

Supplemental material for this article is available online.

References

1. Connolly ES, Jr., Rabinstein AA, Carhuapoma JR, Derdeyn CP, Dion J, Higashida RT, Hoh BL, Kirkness CJ, Naidech AM, Ogilvy CS, Patel AB, et al. Guidelines for the management of aneurysmal subarachnoid hemorrhage: a guideline for healthcare professionals from the American Heart Association/American Stroke Association. Stroke. 2012; 43(6):1711–1737.
2. van Gijn J, Rinkel GJ. Subarachnoid haemorrhage: diagnosis, causes and management. Brain. 2001;124(Pt 2):249–278.
3. Cahill J, Zhang JH. Subarachnoid hemorrhage: is it time for a new direction? Stroke. 2009;40(suppl 3):S86–S87.
4. Fujii M, Yan J, Rolland WB, Soejima Y, Caner B, Zhang JH. Early brain injury, an evolving frontier in subarachnoid hemorrhage research. Transl Stroke Res. 2013;4(4):432–446.
5. Xie Z, Huang L, Enkhjargal B, Reis C, Wan W, Tang J, Cheng Y, Zhang JH. Intranasal administration of recombinant netrin-1 attenuates neuronal apoptosis by activating dcc/appl-1/akt signaling pathway after subarachnoid hemorrhage in rats. Neuropharmacology. 2017;119:123–133.
6. Degterev A, Huang Z, Boyce M, Li Y, Jagtap P, Mizushima N, Cuny GD, Mitchison TJ, Moskowitz MA, Yuan J. Chemical inhibitor of nonapoptotic cell death with therapeutic potential for ischemic brain injury. Nat Chem Biol. 2005;1(2):112–119.
7. Fayaz SM, Suvanish Kumar VS, Rajanikant GK. Necroptosis: who knew there were so many interesting ways to die? CNS Neurol Disord Drug Targets. 2014;13(1):42–51.
8. Su X, Wang H, Kang D, Zhu J, Sun Q, Li T, Ding K. Necrostatin-1 ameliorates intracerebral hemorrhage-induced brain injury in mice through inhibiting rip1/rip3 pathway. Neurochem Res. 2015;40(4):643–650.
9. Wu JR, Wang J, Zhou SK, Yang L, Yin JL, Cao JP, Cheng YB. Necrostatin-1 protection of dopaminergic neurons. Neural Regen Res. 2015;10(7):1120–1124.
10. Liu T, Zhao DX, Cui H, Chen L, Bao YH, Wang Y, Jiang JY. Therapeutic hypothermia attenuates tissue damage and cytokine expression after traumatic brain injury by inhibiting necroptosis in the rat. Sci Rep. 2016;6:24547.
11. Degterev A, Hitomi J, Germscheid M, Ch'en IL, Korkina O, Teng X, Abbott D, Cuny GD, Yuan C, Wagner G, Hedrick SM, et al. Identification of rip1 kinase as a specific cellular target of necrostatins. Nat Chem Biol. 2008;4(5):313–321.
12. Kooijman E, Nijboer CH, van Velthoven CT, Kavelaars A, Kesecioglu J, Heijnen CJ. The rodent endovascular puncture model of subarachnoid hemorrhage: mechanisms of brain damage and therapeutic strategies. J Neuroinflammation. 2014;11:2.
13. Chang P, Dong W, Zhang M, Wang Z, Wang Y, Wang T, Gao Y, Meng H, Luo B, Luo C, Chen X, et al. Anti-necroptosis chemical necrostatin-1 can also suppress apoptotic and autophagic pathway to exert neuroprotective effect in mice intracerebral hemorrhage model. J Mol Neurosci. 2014;52(2): 242–249.
14. You Z, Savitz SI, Yang J, Degterev A, Yuan J, Cuny GD, Moskowitz MA, Whalen MJ. Necrostatin-1 reduces histopathology and improves functional outcome after controlled cortical impact in mice. J Cereb Blood Flow Metab. 2008; 28(9):1564–1573.
15. Northington FJ, Chavez-Valdez R, Graham EM, Razdan S, Gauda EB, Martin LJ. Necrostatin decreases oxidative damage, inflammation, and injury after neonatal hi. J Cereb Blood Flow Metab. 2011;31(1):178–189.
16. Chavez-Valdez R, Flock DL, Martin LJ, Northington FJ. Endoplasmic reticulum pathology and stress response in neurons precede programmed necrosis after neonatal hypoxia-ischemia. Int J Dev Neurosci. 2016;48:58–70.
17. Chen F, Su X, Lin Z, Lin Y, Yu L, Cai J, Kang D, Hu L. Necrostatin-1 attenuates early brain injury after subarachnoid hemorrhage in rats by inhibiting necroptosis. Neuropsychiatr Dis Treat. 2017;13:1771–1782.
18. Zhou K, Shi L, Wang Z, Zhou J, Manaenko A, Reis C, Chen S, Zhang J. RIP1-RIP3-DRP1 pathway regulates NLRP3 inflammasome activation following subarachnoid hemorrhage. Exp Neurol. 2017;295:116–124.
19. Yang C, Li T, Xue H, Wang L, Deng L, Xie Y, Bai X, Xin D, Yuan H, Qiu J, Wang Z, et al. Inhibition of necroptosis rescues SAH-induced synaptic impairments in hippocampus via CREB-BDNF pathway. Front Neurosci. 2018;12:990.
20. Claassen J, Carhuapoma JR, Kreiter KT, Du EY, Connolly ES, Mayer SA. Global cerebral edema after subarachnoid hemorrhage: frequency, predictors, and impact on outcome. Stroke. 2002;33(5):1225–1232.
21. Cahill J, Calvert JW, Zhang JH. Mechanisms of early brain injury after subarachnoid hemorrhage. J Cereb Blood Flow Metab. 2006;26(11):1341–1353.
22. Cao S, Zhu P, Yu X, Chen J, Li J, Yan F, Wang L, Yu J, Chen G. Hydrogen sulfide attenuates brain edema in early brain injury after subarachnoid hemorrhage in rats: possible involvement of MMP-9 induced blood-brain barrier disruption and AQP4 expression. Neurosci Lett. 2016;621:88–97.
23. King MD, Whitaker-Lea WA, Campbell JM, Alleyne CH, Dhandapani KM. Necrostatin-1 reduces neurovascular injury after intracerebral hemorrhage. Int J Cell Biology. 2014;2014: 1–10.
24. Nikseresht S, Khodagholi F, Nategh M, Dargahi L. RIP1 inhibition rescues from LPS-induced RIP3-mediated programmed cell death, distributed energy metabolism and spatial memory impairment. J Mol Neurosci. 2015;57(2):219–230.
25. Park IS, Meno JR, Witt CE, Suttle TK, Chowdhary A, Nguyen TS, Ngai AC, Britz GW. Subarachnoid hemorrhage model in

the rat: modification of the endovascular filament model. J Neurosci Methods. 2008;172(2):195–200.
26. Xu Y, Wang J, Song X, Qu L, Wei R, He F, Wang K, Luo B. RIP3 induces ischemic neuronal DNA degradation and programmed necrosis in rat via AIF. Sci Rep. 2016;6:29362.
27. Yin B, Xu Y, Wei RL, He F, Luo BY, Wang JY. Inhibition of receptor-interacting protein 3 upregulation and nuclear translocation involved in necrostatin-1 protection against hippocampal neuronal programmed necrosis induced by ischemia/reperfusion injury. Brain Res. 2015;1609:63–71.
28. Yan F, Cao S, Li J, Dixon B, Yu X, Chen J, Gu C, Lin W, Chen G. Pharmacological inhibition of perk attenuates early brain injury after subarachnoid hemorrhage in rats through the activation of AKT. Mol Neurobiol. 2017;54(3):1808–1817.
29. Garcia JH, Wagner S, Liu KF, Hu XJ. Neurological deficit and extent of neuronal necrosis attributable to middle cerebral artery occlusion in rats. Statistical validation. Stroke. 1995; 26(4):627–634; discussion 635.
30. Sugawara T, Ayer R, Jadhav V, Zhang JH. A new grading system evaluating bleeding scale in filament perforation subarachnoid hemorrhage rat model. J Neurosci Methods. 2008; 167(2):327–334.
31. Mao S, Xi G, Keep RF, Hua Y. Role of lipocalin-2 in thrombin-induced brain injury. Stroke. 2016;47(4):1078–1084.
32. Ni W, Zheng M, Xi G, Keep RF, Hua Y. Role of lipocalin-2 in brain injury after intracerebral hemorrhage. J Cereb Blood Flow Metab. 2015;35(9):1454–1461.
33. Okubo S, Strahle J, Keep RF, Hua Y, Xi G. Subarachnoid hemorrhage-induced hydrocephalus in rats. Stroke. 2013; 44(2):547–550.
34. Guo D, Wilkinson DA, Thompson BG, Pandey AS, Keep RF, Xi G, Hua Y. MRI characterization in the acute phase of experimental subarachnoid hemorrhage. Transl Stroke Res. 2017;8(3):234–243.
35. Chen J, Wang L, Wu C, Hu Q, Gu C, Yan F, Li J, Yan W, Chen G. Melatonin-enhanced autophagy protects against neural apoptosis via a mitochondrial pathway in early brain injury following a subarachnoid hemorrhage. J Pineal Res. 2014; 56(1):12–19.
36. Wu Y, Wang YP, Guo P, Ye XH, Wang J, Yuan SY, Yao SL, Shang Y. A lipoxin a4 analog ameliorates blood-brain barrier dysfunction and reduces MMP-9 expression in a rat model of focal cerebral ischemia-reperfusion injury. J Mol Neurosci. 2012;46(3):483–491.
37. Xu H, Li J, Wang Z, Feng M, Shen Y, Cao S, Li T, Peng Y, Fan L, Chen J, Gu C, et al. Methylene blue attenuates neuroinflammation after subarachnoid hemorrhage in rats through the AKT/GSK-3beta/MEF2D signaling pathway. Brain Behav Immun. 2017;65:125–139.
38. Yang Y, Estrada EY, Thompson JF, Liu W, Rosenberg GA. Matrix metalloproteinase-mediated disruption of tight junction proteins in cerebral vessels is reversed by synthetic matrix metalloproteinase inhibitor in focal ischemia in rat. J Cereb Blood Flow Metab. 2007;27(4):697–709.
39. Egashira Y, Zhao H, Hua Y, Keep RF, Xi G. White matter injury after subarachnoid hemorrhage: role of blood-brain barrier disruption and matrix metalloproteinase-9. Stroke. 2015;46(10):2909–2915.
40. Pierdomenico M, Negroni A, Stronati L, Vitali R, Prete E, Bertin J, Gough PJ, Aloi M, Cucchiara S. Necroptosis is active in children with inflammatory bowel disease and contributes to heighten intestinal inflammation. Am J Gastroenterol. 2014; 109(2):279–287.
41. Jia Z, Xu C, Shen J, Xia T, Yang J, He Y. The natural compound celastrol inhibits necroptosis and alleviates ulcerative colitis in mice. Int Immunopharmacol. 2015;29(2):552–559.
42. Xie T, Peng W, Liu Y, Yan C, Maki J, Degterev A, Yuan J, Shi Y. Structural basis of RIP1 inhibition by necrostatins. Structure. 2013;21(3):493–499.
43. Wang K, Li J, Degterev A, Hsu E, Yuan J, Yuan C. Structure-activity relationship analysis of a novel necroptosis inhibitor, necrostatin-5. Bioorg Med Chem Lett. 2007;17(5):1455–1465.
44. Zheng W, Degterev A, Hsu E, Yuan J, Yuan C. Structure-activity relationship study of a novel necroptosis inhibitor, necrostatin-7. Bioorg Med Chem Lett. 2008;18(18): 4932–4935.
45. Chen J, Chen G, Li J, Qian C, Mo H, Gu C, Yan F, Yan W, Wang L. Melatonin attenuates inflammatory response-induced brain edema in early brain injury following a subarachnoid hemorrhage: a possible role for the regulation of pro-inflammatory cytokines. J Pineal Res. 2014;57(3):340–347.
46. Li J, Chen J, Mo H, Chen J, Qian C, Yan F, Gu C, Hu Q, Wang L, Chen G. Minocycline protects against nlrp3 inflammasome-induced inflammation and p53-associated apoptosis in early brain injury after subarachnoid hemorrhage. Mol Neurobiol. 2016;53(4):2668–2678.
47. Chou SH, Feske SK, Simmons SL, Konigsberg RG, Orzell SC, Marckmann A, Bourget G, Bauer DJ, De Jager PL, Du R, Arai K, et al. Elevated peripheral neutrophils and matrix metalloproteinase 9 as biomarkers of functional outcome following subarachnoid hemorrhage. Transl Stroke Res. 2011;2(4): 600–607.
48. He S, Wang L, Miao L, Wang T, Du F, Zhao L, Wang X. Receptor interacting protein kinase-3 determines cellular necrotic response to TNF-alpha. Cell. 2009;137(6):1100–1111.
49. Linkermann A, Green DR. Necroptosis. N Engl J Med. 2014; 370(5):455–465.
50. Sun L, Wang H, Wang Z, He S, Chen S, Liao D, Wang L, Yan J, Liu W, Lei X, Wang X. Mixed lineage kinase domain-like protein mediates necrosis signaling downstream of RIP3 kinase. Cell. 2012;148(1–2):213–227.
51. Wang H, Sun L, Su L, Rizo J, Liu L, Wang LF, Wang FS, Wang X. Mixed lineage kinase domain-like protein MLKL causes necrotic membrane disruption upon phosphorylation by RIP3. Mol Cell. 2014;54(1):133–146.
52. Jing CH, Wang L, Liu PP, Wu C, Ruan D, Chen G. Autophagy activation is associated with neuroprotection against apoptosis via a mitochondrial pathway in a rat model of subarachnoid hemorrhage. Neuroscience. 2012;213:144–153.
53. Gaetani P, Tartara F, Pignatti P, Tancioni F, Rodriguez y Baena R, De Benedetti F. Cisternal CSF levels of cytokines after subarachnoid hemorrhage. Neurol Res. 1998;20(4):337–342.

54. Mathiesen T, Andersson B, Loftenius A, von Holst H. Increased interleukin-6 levels in cerebrospinal fluid following subarachnoid hemorrhage. J Neurosurg. 1993;78(4): 562–567.
55. Mathiesen T, Edner G, Ulfarsson E, Andersson B. Cerebrospinal fluid interleukin-1 receptor antagonist and tumor necrosis factor-alpha following subarachnoid hemorrhage. J Neurosurg. 1997;87(2):215–220.
56. Sozen T, Tsuchiyama R, Hasegawa Y, Suzuki H, Jadhav V, Nishizawa S, Zhang JH. Role of interleukin-1beta in early brain injury after subarachnoid hemorrhage in mice. Stroke. 2009;40(7):2519–2525.
57. Moriwaki K, Chan FK. Necroptosis-independent signaling by the RIP kinases in inflammation. Cell Mol Life Sci. 2016; 73(11–12):2325–2334.
58. Pang J, Chen Y, Kuai L, Yang P, Peng J, Wu Y, Chen Y, Vitek MP, Chen L, Sun X, Jiang Y. Inhibition of blood-brain barrier disruption by an apolipoprotein e-mimetic peptide ameliorates early brain injury in experimental subarachnoid hemorrhage. Transl Stroke Res. 2017;8(3):257–272.
59. Qin W, Lu W, Li H, Yuan X, Li B, Zhang Q, Xiu R. Melatonin inhibits IL1beta-induced MMP9 expression and activity in human umbilical vein endothelial cells by suppressing NF-kappab activation. J Endocrinol. 2012;214(2):145–153.
60. Chen J, Qian C, Duan H, Cao S, Yu X, Li J, Gu C, Yan F, Wang L, Chen G. Melatonin attenuates neurogenic pulmonary edema via the regulation of inflammation and apoptosis after subarachnoid hemorrhage in rats. J Pineal Res. 2015; 59(4):469–477.
61. Wessell AP, Kole MJ, Cannarsa G, Oliver J, Jindal G, Miller T, Gandhi D, Parikh G, Badjatia N, Aldrich EF, Simard JM. A sustained systemic inflammatory response syndrome is associated with shunt-dependent hydrocephalus after aneurysmal subarachnoid hemorrhage. J Neurosurg. Epub ahead of print 1 June 2018. DOI: 10.3171/2018.1.JNS172925.
62. Chen S, Luo J, Reis C, Manaenko A, Zhang J. Hydrocephalus after subarachnoid hemorrhage: pathophysiology, diagnosis, and treatment. BioMed Res Int. 2017;2017:8584753.
63. Karimy JK, Zhang J, Kurland DB, Theriault BC, Duran D, Stokum JA, Furey CG, Zhou X, Mansuri MS, Montejo J, Vera A, et al. Inflammation-dependent cerebrospinal fluid hypersecretion by the choroid plexus epithelium in posthemorrhagic hydrocephalus. Nat Med. 2017;23(8):997–1003.
64. Fang Y, Chen S, Reis C, Zhang J. The role of autophagy in subarachnoid hemorrhage: an update. Curr Neuropharmacol. 2018;16(9):1255–1266.
65. Cook WD, Moujalled DM, Ralph TJ, Lock P, Young SN, Murphy JM, Vaux DL. RIPK1- and RIPK3-induced cell death mode is determined by target availability. Cell Death Differ. 2014;21(10):1600–1612.
66. Mandal P, Berger SB, Pillay S, Moriwaki K, Huang C, Guo H, Lich JD, Finger J, Kasparcova V, Votta B, Ouellette M, et al. RIP3 induces apoptosis independent of pronecrotic kinase activity. Mol Cell. 2014;56(4):481–495.
67. Goodall ML, Fitzwalter BE, Zahedi S, Wu M, Rodriguez D, Mulcahy-Levy JM, Green DR, Morgan M, Cramer SD, Thorburn A. The autophagy machinery controls cell death switching between apoptosis and necroptosis. Dev Cell. 2016;37(4): 337–349.